Nanometric Precision Distance Metrology via Hybrid Spectrally Resolved and Homodyne Interferometry in a Single Soliton Frequency Microcomb

Yoon-Soo Jang, Hao Liu, Jinghui Yang, Mingbin Yu, Dim-Lee Kwong, and Chee Wei Wong

Phys. Rev. Lett. **126**, 023903 — Published 14 January 2021

DOI: 10.1103/PhysRevLett.126.023903

Nanometric precision distance metrology via hybrid spectrally-resolved and homodyne interferometry in a single soliton frequency microcomb

Yoon-Soo Jang,[1,2,†,*], Hao Liu,[1,†] Jinghui Yang,[1] Mingbin Yu,[3] Dim-Lee Kwong,[3] and Chee Wei Wong,[1*]

[1] Fang Lu Mesoscopic Optics and Quantum Electronics Laboratory, University of California, Los Angeles, CA 90095, USA.

[2] Length Standards Group, Division of Physical Metrology, Korea Research Institute of Standards and Science (KRISS), 267 Gajeong-ro, Yuseong-gu, Daejeon, 34113, Republic of Korea.

[3] Institute of Microelectronics, Singapore 117685, Singapore.

[†] These authors contributed equally to this work.

* ysj@kriss.re.kr; cheewei.wong@ucla.edu

Laser interferometry serves a fundamental role in science and technology, assisting precision metrology and dimensional length measurement. During the past decade, laser frequency combs – a coherent optical-microwave frequency ruler over a broad spectral range with traceability to time-frequency standards – have contributed pivotal roles in laser dimensional metrology with ever-growing demands in measurement precision. Here we report spectrally-resolved laser dimensional metrology via a free-running soliton frequency microcomb, with nanometric-scale precision. Spectral interferometry provides information on the optical time-of-flight signature, and the large free-spectral range and high-coherence of the microcomb enable tooth-resolved and high-visibility interferograms that can be directly readout with optical spectrum instrumentation. We employ a hybrid timing signal from comb-line homodyne, microcomb, and background amplified spontaneous emission spectrally-resolved interferometry – all from the same spectral interferogram. Our combined soliton and homodyne architecture demonstrates a 3-nm repeatability over a 23-mm non-ambiguity range achieved via homodyne interferometry, and over 1,000-seconds stability in the long-term precision metrology at the white noise limits.

Introduction

With length as one of seven fundamental physical quantities, the ability to precisely determine distance to a target is especially important such as in observations of gravitational waves [1] and futuristic space missions of multiple satellite flying formations [2]. With the current international system of units (SI) meter definition based on light vacuum path traveled in a time of 1/299,792,458 second [3,4], laser-based distance measurement plays a pivotal role to advance length metrology with increasing precision. Most laser interferometers are based on the single-wavelength, with interferometric phase measurement to achieve sub-wavelength precision [5]. Inherently, a single-wavelength laser interferometer measures distance by accumulating a displacement from the initial to the target position, with the non-ambiguity range bounded at half the selected electromagnetic wavelength. To overcome this limitation, absolute distance measurement – which determines distance by a single operation – has been advanced in various platforms [6-10].

The advent of the frequency comb, which enables the whole optical frequency span to have traceability to well-defined frequency standards in the microwave or optical domains [11-13], brought about a breakthrough in absolute distance measurements [14]. The broad spectrum and ultrashort pulse of the frequency comb enable advanced laser distance metrology including dual-comb interferometry [8,15], synthetic-wavelength interferometry [16-18], spectrally-resolved interferometry [19-22], multi-wavelength interferometry [23-25], and cross-correlated time-of-flight measurements [9,26]. Recently chip-scale microresonators have contributed to progress in laser frequency combs [27-30] including the generation of different frequency microcombs [31-35] temporal solitons [36,37], integrated low-power microcombs [38], and optical frequency synthesizers [39]. These microcombs enable applications such as low-noise microwave generation [40,41], optical communications [42], spectroscopy [43,44], and distance measurement at ≈ 100 nm precision [45-47].

Here we describe spectrally-resolved laser ranging via a soliton frequency microcomb, with precision length metrology at the few nanometers scale. A single microcomb is utilized, of which the spectrally-resolved interferometry (SRI) of the measurement and reference pulses engraves information on the optical time-of-flight. With the large (88.5-GHz) free-spectral range and high-

coherence of our selected frequency microcomb, we directly read out the tooth-resolved and high-visibility interferogram via optical spectrum analyzers. We utilize a dual-pumping technique to stably generate the soliton mode-locking in a planar-waveguide Si_3N_4 microresonator [48]. We describe the time-of-flight signal reconstruction via the integrated platform of comb-line homodyne interferometry, microcomb and background amplified spontaneous emission spectrally-resolved interferometry, from the same spectral interferogram. The comb-line homodyne interferometry is unwrapped with the relatively-coarse microcomb, which is itself unwrapped with the low-coherence amplified spontaneous emission interferometry in the comb-background to achieve a 3-nm precision over a 23-mm non-ambiguity range. We sample the long-term distance metrology over 1,000-seconds stability and an Allan deviation up to 300-seconds, with a 3-nm measurement repeatability achieved from homodyne interferometry. The chip-scale single microcomb provides a platform to apply a hybrid microcomb and homodyne spectrally-resolved interferometry architecture, achieving white noise-bounded high precision at long integration times and short distances, even comparable to a few-Hz stabilized fiber frequency combs. We further demonstrate measurement linearity in example positional calibration and referenced against a three-dimensional (3D) precision gauge block for principle demonstration.

Measurement concept of soliton microcomb ranging by spectrally-resolved interferometry

Figure 1 shows our laser dimensional measurement concept with the soliton frequency microcomb. The time-delayed measurement pulse is described by relative phase delay $\varphi(\nu)$ (= $2\pi\nu \times \tau_{TOF}$) to the reference pulse, with ν the optical carrier and τ_{TOF} the measurement-reference time-of-flight delay. With $s(\nu)$ the pulse spectrum, two separated pulses generate a frequency interference pattern as $i(\nu) = s(\nu)\,[1 + \cos\varphi(\nu)]$, engraving the time delay with $1/\tau_{TOF}$ period (Fig. 1 right panel) with target distance L determination from $2n_{air}L = (c_o\tau_{TOF})$ where c_o is the vacuum speed of light and n_{air} the medium refractive index. The time delay τ_{TOF} is directly determined by the peak position of the $i(\nu)$ Fourier-transform, expressed as $I(\tau) = FT\{i(\nu)\} = S(\tau) \otimes [\delta(\tau+\tau_{TOF})/2 + \delta(\tau) + \delta(\tau-\tau_{TOF})/2]$, where $\delta(\tau)$ is the Dirac delta function, $S(\tau)$ the $s(\nu)$ Fourier transform, and τ the time delay. Since $s(\nu)$ is a real function, its Fourier transform $S(\tau)$ is symmetric about $\tau = 0$ and repeated every $\tau = \tau_{pp}$ (=$1/f_r$), where f_r is the repetition-rate and τ_{pp} the pulse-to-pulse temporal separation.

Since the τ_{TOF} peak is symmetrical to $\tau_{pp}/2$, the measured τ_{TOF} folds at $\tau_{pp}/2$ and the measured distance has a triangle-shaped profile with increasing target distance [19]. Thus the target distance is expressed as $2n_{air}L = c_o(m\times\tau_{pp}/2 + \tau_{TOF})$ for even m, or $2n_{air}L = c_o\{(m+1)\times\tau_{pp}/2 - \tau_{TOF}\}$ for odd m, where m is an integer. In general, the calculated τ_{TOF} from $S(\tau)$ peak detection is not precisely determined and is limited by the $s(v)$ bandwidth. We use a curve-fitting algorithm for precision peak detection and homodyne interferometry toward nanometer-level precision, with further details in Supplementary Materials S1 [57]. Note that the non-ambiguity range (L_{NAR}) is determined from f_r [$L_{NAR} = c/(4f_r)$] which corresponds to 850-μm (f_r = 88.5 GHz). For further precise measurement, we use the optical carrier phase from the inverse Fourier transformation of $S(\tau)$. Then the target distance can be defined as $2n_{air}L = c_o/v(M_{homodyne} + \square(v))$, where $M_{homodyne}$ is the integer of the homodyne interferometry.

Figure 2 depicts the setup for the microcomb-based dimensional metrology. A dissipative single-soliton is generated in a planar Si_3N_4 microresonator, with loaded quality-factor Q of 1.77×10^6, free spectral range (FSR) of 88.5 GHz, and anomalous group velocity dispersion β_2 of -3 ± 1.1 fs^2/mm at 1595-nm. The stable single-soliton microcomb mode-locking is achieved with a counter-propagating dual-driven technique (see Supplementary Materials S2). Fig. 2(b) shows the generated single-soliton microcomb, formed in the microresonator with Kerr nonlinearity. The soliton microcomb has a hyperbolic secant-square shape with a 1595-nm center wavelength and a 40-nm bandwidth. Such a broad spectrum fits well with SRI since the minimum measurable distance (L_{min}) is limited by the Fourier-transform limited pulse duration of light source (τ_{pulse}) as $2L_{min} = c_o\times\tau_{pulse}$ [19]. The right inset of Fig. 2(b) shows the repetition rate (f_r) frequency stability Allan deviation, at about 5×10^{-8} level between 0.5 to 100-seconds (detailed in Supplementary Materials S3).

Figure 2(a) shows the experimental setup for absolute distance measurement. A C-band section of the soliton comb is first amplified with an erbium-doped fiber amplifier up to 10 mW, centered at 192-THz with 2-THz bandwidth. A 50:50 beam splitter divides the soliton microcomb pulses into the reference and measurement arms for the interferometry and recombines upon the pulses return. The measurement mirror (M_{Mea}) is mounted on a motorized stage for translational motion. The recombined beam is collimated into a single-mode fiber, and sent into an optical spectrum analyzer with 50-pm resolution and 10-pm accuracy (or

equivalently 6.3×10^{-6} wavelength inaccuracy with respect to the optical electromagnetic carrier). An example resulting spectral interference pattern is shown in the blue plot of Fig. 2(c). Since the microcomb has a large 88.5-GHz repetition-rate, the comb tooth-resolved interferogram can be directly read out with optical spectrum analyzer. In contrast, conventional fiber frequency combs rely on Fabry-Perot etalon-based mode filtering or virtually-imaged phase array spectrometers for comb tooth-resolved spectrograms. In Fig. 2(c), the background gray spectrum is the amplified C-band section of the original soliton microcomb for reference.

Absolute distance metrology by soliton microcomb-based spectrally-resolved interferometry

To evaluate the measurement reliability, we measured a fixed distance over 1,000-seconds with a 1-second update rate. During the measurements, the air refractive index is fixed at 1.000247, which is calculated by the empirical equation under standard air [49]. Since the non-ambiguity range of microcomb-based SRI is limited by hundreds of micrometer, we extend the non-ambiguity range by introducing coarse measurement from ASE spectrum-based SRI [50,51]. Since the spectrometer resolution is 50-pm ($\delta\nu_{\text{spectrometer}}$ = 6.14-GHz at 1560-nm), the maximum measurable range of ASE spectrum-based SRI ($L_{\text{MAX\_ASE}}$) is 23.4-mm by relation of $L_{\text{MAX\_ASE}} = c_o/2n\delta\nu_{\text{spectrometer}}$. Further measurement range extension can be realized by introducing other coarse distance metrology [20,25]. As shown in Fig. 3(b), the target distance ($L_{\text{Mea}} = c_o\tau_{\text{TOF}}/2$) and non-ambiguity range ($L_{\text{NAR}} = c_o\tau_{\text{pp}}/4$) is determined from the reconstructed time-domain signal, based on Fourier transform of the interference pattern in the frequency domain. Fig. 3(b) shows the non-ambiguity range at 0.847424-mm. We see a large peak enhanced by summation of the ASE and microcomb spectrum, extending the measurement range.

We evaluate the measurement linearity by comparing with the encoder inside the motorized stage as shown in Fig. 3(c). As shown in Fig. 3(c-1), we model the positioning error with 3 types of spectral shapes with ideal interference pattern on the spectrum. Although amplified comb spectrum is narrower than original soliton microcomb spectrum, the positioning error of amplified comb spectrum case is better because of its smooth spectrum shape. The positioning errors of amplified comb, full microcomb and sech^2 spectrum with same spectral bandwidth of amplified comb are estimated with standard deviations (1σ) of 124-nm, 560-nm and 23-nm, respectively. The measurements revealed a peak-to-valley discrepancy of ± 2.56-μm. We note

that the comparison is limited by the motorized stage due to its low accuracy (≈ ± 5-μm) (see Supplementary Materials S4). For further comparison, we compare the measurements between microcomb SRI and homodyne interferometry. The peak-to-valley discrepancy is ± 293-nm with standard deviation (1σ) of 185-nm. We also evaluated the translation motion exceeding the non-ambiguity range of 850-μm as shown in Fig. 3(c) inset. For comparison, the fiber comb-based SRI result is also plotted in light cyan. Beyond the non-ambiguity range, our measurement and the encoder matches well within the encoder accuracy. We also measured a standardized gauge block cross-section with 3-mm height to validate the microcomb SRI for potential 3D surface measurement. The measurement repeatability taken over 5 consecutive measurements is determined to be 327-nm and 11.4-nm from microcomb SRI and homodyne interferometry respectively as the 1σ standard deviation (detailed in Supplementary Materials S5). These results demonstrate that the microcomb SRI has a good potential for length and positioning calibration such as length standards and high-precision axial positioning.

As shown in Fig. 4(a) and 4(b) up to 1,000-seconds, the measured distance from microcomb SRI is nearly constant without notable long-term drifts and has a standard deviation (1σ) of 81.6-nm. In contrast, the ASE spectrum-based SRI shows large fluctuations in the distance measurement due to its incoherence, but aids to extend the measurement range via non-commensurate periods in the time-domain. The ASE spectrum-based SRI measurement range is instead usually limited by the spectrometer optical resolution. An average value of the measured distance from microcomb-based SRI is found to be 8.197951-mm, and its accuracy is estimated to be 52-nm bounded by the optical spectrum analyzer. This accuracy can be enhanced by precisely measuring the repetition-rate f_r, instead of reading out solely the spectrum analyzer values. Measurement repeatability (in terms of Allan deviation) is calculated via the long-term measurement as shown in Fig. 4(c). As noted in Fig. 4(c), the measurement repeatability of microcomb-based SRI at 1-second (without averaging) is found to be 80-nm. The measurement repeatability gradually improves to 11-nm, with a measurement fitted relation of 80-nm × $\tau_{avg}^{-0.5}$. For longer averaging time more than 10-seconds, the measurement repeatability remains below 20-nm.

Homodyne interferometry provides a complementary approach to further improve the distance metrology precision at the nanometric level, since it employs the optical carrier frequency instead of the pulse train envelope in microcomb ranging. Using multiple comb lines,

our comb-based homodyne interferometry counts the optical carrier phase and its measured distance has a standard deviation (1σ) of 10.4-nm during the 1,000-seconds integration. We observed slowly-varying fluctuations (random walk), as shown in Fig. 4(a). (We note that for specific ranges, such as 900 to 1,000-seconds in this case, the standard deviation improves to 3.6-nm.) An average value of the measured distance from homodyne interferometry is found to be 8.197915-mm. As shown in Fig. 4(c), the measurement repeatability of homodyne interferometry at 1-second is found to be 2.85-nm which deteriorated to 6.62-nm at 100-seconds. The measurement repeatability of microcomb-based SRI and homodyne interferometry are overlapping at more than 100-seconds of averaging because it is perhaps bounded by slowly-varying fluctuations on the optical path delay due to measurement path thermal expansion, air refractive index variations by slowly-varying environmental drift, or long-term fluctuations of the measured spectrum. If we remove long-term drift using high-pass filtering, the measurement stability can be enhanced to sub-nm at 100-seconds averaging as shown Supplementary Materials Fig. S6 (detailed in Supplementary Materials S6). We compare our soliton microcomb stability measurements with a fully-stabilized fiber frequency comb reference in the SRI (detailed in Supplementary Materials S7). The measurement repeatability is well-matched to each other, verifying that our measurement stability is not limited by the soliton microcomb. We note that the main limitations on the repeatability is the intensity fluctuations such as from the spectrum analyzer, microcomb, polarization and distance variations and is further described in Supplementary Materials S8.

We have examined the scaling of the microcomb SRI with estimates of the microcomb stability (detailed in Figure S8). For distances smaller than 1-m, our precision limit is bounded by the measurement repeatability. For distances more than 1-m, the measurement precision will be bounded by the frequency stability of our free-running frequency microcomb which has been reported at the 10^{-8} to 10^{-9} level [52]. The scaling is square-root proportional with distance since for the longer distances the precision limit is bounded by the microcomb frequency instability ($\Delta f/f \sim \Delta L/L$). When locking the free-running microcomb to a Rb atomic clock or micro-photonic reference [53-56], the frequency stability can be brought down to 10^{-12} at 100-seconds integration, further improving the long-distance precision of the single-soliton microcomb spectrally-resolved interferometry. Our proposed scheme can be a platform for next-generation length standards via chip-scale laser frequency microcombs.

Acknowledgments

The authors acknowledge discussions with Ki-Nam Joo, Abhinav Kumar Vinod, Wenting Wang, Jinkang Lim, Ken Chih-Kong Yang, and Li-Yang Chen. The authors acknowledge support from the Office of Naval Research (N00014-16-1-2094), the Lawrence Livermore National Laboratory (contract B622827), and the National Science Foundation. Y.-S.J. acknowledges support of the Korea Research Institute of Standards and Science (20011030). Y.-S. J. designed and led the work. H. L. led the soliton generation. Y.-S. J. performed distance measurements. J. Y., M. Y. and D.-L. K. nanofabricated the microresonator. Y.-S. J. and C. W. W. performed the measured data analysis. All authors discussed the results. Y.-S. J. and C.W.W. prepared the manuscript.

References

1. B. P. Abbott et al. (LIGO Scientific Collaboration and Virgo Collaboration) , Observation of gravitational waves from a binary black hole merger, *Phys. Rev. Lett.* **116**, 061102 (2016).
2. D. Massonnet, M. Rossi, C. Carmona, F. Adragna, G. Peltzer, K. Feigl, and T. Rabaute, The displacement field of the Landers earthquake mapped by radar interferometry, *Nature* **364**, 138-142 (1993).
3. P. Giacomo, News from the BIPM, *Metrologia* **20**, 25–30 (1984).
4. S. A. Diddams, J. C. Bergquist, S. R. Jefferts, and C. W. Oates, Standards of time and frequency at the outset of the 21st century, *Science* **306**, 1318-1324 (2004).
5. N. Bobroff, Recent advances in displacement measuring interferometry, *Meas. Sci. Technol.* **4**, 907–926 (1993).
6. P. L. Bender, D. G. Currie, S. K. Poultney, C. O. Alley, R. H. Dicke, D. T. Wilkinson, D. H. Eckhardt, J. E. Faller, W. M. Kaula, J. D. Mulholland, H. H. Plotkin, E. C. Silverberg, J. G. Williams, The lunar laser ranging experiment, *Science* **182**, 229 (1973).
7. I. Fujima, S. Iwasaki, and K. Seta, High-resolution distance meter using optical intensity modulation at 28 GHz, *Meas. Sci. Technol.* **9**, 1049 (1998).
8. I. Coddington, W.C. Swann, L. Nenadovic, and N. R. Newbury, Rapid and precise absolute distance measurements at long range, *Nat. Photon.* **3**, 351-356 (2009).
9. J. Lee, Y.-J. Kim, K. Lee, S. Lee, and S.-W. Kim, Time-of-flight measurement using femtosecond light pulses, *Nat. Photon*. **4**, 716-720 (2010).
10. W. Gao, S.-W. Kim, H. Bosse, H. Haitjema, Y. L. Chen, X. D. Lu, W. Knapp, A. Weckenmann, W. T. Estler, and H. Kunzmann, Measurement technologies for precision positioning, *CIRP Ann. Manuf. Technol.* **64**, 773–796 (2015).

11. D. J. Jones, S. A. Diddams, J. K. Ranka, A. Stentz, R. S. Windeler, J. L. Hall, and S. T. Cundiff, Carrier-envelope phase control of femtosecond mode-locked lasers and direct optical frequency synthesis, *Science* **288**, 635-639 (2000).

12. S. A. Diddams, D. J. Jones, J. Ye, S. T. Cundiff, and J. L. Hall, Direct link between microwave and optical frequencies with a 300 THz femtosecond laser comb, *Phys. Rev. Lett.* **84**, 5102-5105 (2000).

13. T. Udem, R. Holzwarth, and T. W. Hänsch, Optical frequency metrology, *Nature* **416**, 233-237 (2002).

14. S.-W. Kim, Metrology: combs rule, *Nat. Photon.* **3**, 313–314 (2009).

15. T.-A. Liu, N. R. Newbury, and I. Coddington, Sub-micron absolute distance measurements in sub-millisecond times with dual free-running femtosecond Er fiber-lasers, *Opt. Express* **19**, 18501–18509 (2011).

16. K. Minoshima and H. Matsumoto, High-accuracy measurement of 240-m distance in an optical tunnel by use of a compact femtosecond laser, *Appl. Opt.* **69**, 5512–5517 (2000).

17. N. R. Doloca, K. Meiners-Hagen, M. Wdeed, F. Pollinger, and A. Abou-Zeid, Absolute distance measurement system using a femtosecond laser as a modulator, *Meas. Sci. Technol.* **21**, 115302 (2010).

18. Y.-S. Jang, W. Kim, H. Jang, and S.-W. Kim, Absolute distance meter operating on a free-running mode-locked laser for space mission, *Int. J. Precis. Eng. Manuf.* **19**, 975-981 (2018).

19. K.-N. Joo and S.-W. Kim, Absolute distance measurement by dispersive interferometry using a femtosecond pulse laser, *Opt. Express* **14**, 5954-5960 (2006).

20. K.-N. Joo, Y. Kim, and S.-W. Kim, Distance measurements by combined method based on a femtosecond pulse laser, *Opt. Express* **16**, 19799-19806 (2008).

21. S. A. van den Berg, S. T. Persijn, G. J. P. Kok, M. G. Zeitouny, and N. Bhattacharya, Many-wavelength interferometry with thousands of lasers for absolute distance measurement, *Phys. Rev. Lett.* **108**, 183901 (2012).

22. A. Lešundák, D. Voigt, O. Cip, and S. A. van den Berg, High-accuracy long distance measurements with a mode-filtered frequency comb, *Opt. Express* **25**, 32570-32580 (2017).

23. N. Schuhler, Y. Salvadé, S. Lévêque, R. Dändliker, and R. Holzwarth, Frequency-comb-referenced two-wavelength source for absolute distance measurement, *Opt. Lett.* **31**, 3101–3103 (2006).

24. G. Wang, Y.-S. Jang, S. Hyun, B. J. Chun, H. J. Kang, S.,Yan, S.-W. Kim, and Y.-J. Kim, Absolute positioning by multi-wavelength interferometry referenced to the frequency comb of a femtosecond laser, *Opt. Express* **23**, 9121-9129 (2015).

25. Y.-S. Jang, G. Wang, S. Hyun, B. J. Chun, H. J. Kang, Y.-J. Kim, and S.-W. Kim, Comb-referenced laser distance interferometer for industrial nanotechnology, *Sci. Rep.* **6**, 31770 (2016).

26. H. Shi, Y. Song, F. Liang, L. Xu, M. Hu, and C. Wang, Effect of timing jitter on time-of-flight distance measurements using dual femtosecond lasers, *Opt. Express* **23**, 14057-14069 (2015).

27. T. J. Kippenberg, R. Holzwarth, and S. A. Diddams, Microresonator-based optical frequency combs, *Science* **332**, 555-559 (2011).

28. S.-W. Huang, H. Zhou, J. Yang, J. F. McMillan, A. Matsko, M. Yu, D.-L. Kwong, L. Maleki, and C. W. Wong, Mode-locked ultrashort pulse generation from on-chip normal dispersion microresonators, *Phys. Rev. Lett.* **114**, 053901 (2015).

29. S.-W. Huang, J. Yang, S.-H. Yang, M. Yu, D.-L. Kwong, T. Zelevinsky, M. Jarrahi, and C. W. Wong, Globally Stable Microresonator Turing Pattern Formation for Coherent High-Power THz Radiation On-Chip, *Phys. Rev. X* **7**, 041002 (2017).

30. T. J. Kippenberg, A. L. Gaeta, M. Lipson, and M. L. Gorodetsky, Dissipative Kerr solitons in optical microresonators, *Science* **361**, eaan8083 (2018).

31. P. Del Haye, A. Schliesser, O. Arcizet, T. Wilken, R. Holzwarth, and T. J. Kippenberg, Optical frequency comb generation from a monolithic microresonator, *Nature* **450**, 1214–1217 (2007).

32. X. Xue, Y. Xuan, Y. Liu, P. Wang, S. Chen, J. Wang, D. Leaird, M. Qi, and A. Weiner, Mode-locked dark pulse Kerr combs in normal-dispersion microresonators, *Nat. Photon.* **9**, 594–600 (2015).

33. B. C. Yao, S.-W. Huang, Y. Liu, A. K. Viniod, C. Choi, M. Hoff, Y. Li, M. Yu, Z. Feng, D.-L. Kwong, Y. Huang, Y. Rao, X. Duan, and C. W. Wong, Gate-tunable frequency combs in graphene-nitride microresonators, *Nature* **558**, 410-414 (2018).

34. J. Yang, S.-W. Huang, Z. Xie, M. Yu, D.-L. Kwong, and C. W. Wong, Coherent satellites in multispectral regenerative frequency microcombs, *Comm. Phys.* **3**, 27 (2020).

35. J. Liu, H. Tian, E. Lucas, A. S. Raja, G. Lihachev, R. N. Wang, J. He, T. Liu, M. H. Anderson, W. Weng, S. A. Bhave, and T. J. Kippenberg, Monolithic piezoelectric control of soliton microcombs, *Nature* **583**, 385-390 (2020).

36. T. Herr, V. Brasch, J. Jost, C. Wang, N. Kondratiev, M. L. Gorodetsky, and T. J. Kippenberg, Temporal solitons in optical microresonators, *Nat. Photon.* **8**, 145–152 (2014).

37. Q. F. Yang, X. Yi, K. Y. Yang, and K. J. Vahala, Counter-propagating solitons in microresonators, *Nat. Photon.* **11**, 560-564 (2017).

38. B. Stern, X. Ji, Y. Okawachi, A. L. Gaeta, and M. Lipson, Battery-operated integrated frequency comb generator, *Nature* **562**, 401-405 (2018).

39. D. T. Spencer, T. Drake, T. C. Briles, J. Stone, L. C. Sinclair, C. Fredrick, Q. Li, D. Westly, B. R. Ilic, A. Bluestone, N. Volet, T. Komljenovic, L. Chang, S. H. Lee, D. Y. Oh, M.-G. Suh, K. Y. Yang, M. H. P. Pfeiffer, T. J. Kippenberg, E. Norberg, L. Theogarajan, K. Vahala, N. R. Newbury, K. Srinivasan, J. E. Bowers, S. A. Diddams, and S. B. Papp, An optical-frequency synthesizer using integrated photonics, *Nature* **557**, 81-85 (2018).

40. J. Liu, E. Lucas, AS. Raja, J. Riemensberger, R.N. Wang, M. Karpov, H. Guo, R. Bouchand and T.J. Kippenberg, Photonic microwave generation in the X- and K-band using integrated soliton microcombs, *Nat. Photonics* **14**, 486–491 (2020).

41. W. Liang, D. Eliyahu, V. S. Ilchenko, A. A. Savchenkov, A. B. Matsko, D. Seidel, and L. Maleki, High spectral purity Kerr frequency comb radio frequency photonic oscillator, *Nat. Commun.* **6**, 7957 (2015).

42. P. Marin-Palomo, J. N. Kemal. M. Karpov, A. Kordts, J. Pfeifle, M. H. P. Pfeiffer, P. Trocha, S. Wolf, V. Brasch, M. H. Anderson, R. Rosenberger, K. Vijayan, W. Freude, T. J. Kippenberg, and C. Koos, Microresonator-based solitons for massively parallel coherent optical communications, *Nature* **546**, 274-279 (2017).

43. M.-G. Suh, Q.-F. Yang, K. Y. Yang, X. Yi, and K. J. Vahala, Microresonator soliton dual-comb spectroscopy, *Science* **354**, 600–603 (2016).

44. A. Dutt, C. Joshi, X. Ji, J. Cardenas, Y. Okawachi, K. Luke, A. L. Gaeta, and M. Lipson, On-chip dual-comb source for spectroscopy, *Sci. Adv.* **4**, e1701858 (2018).

45. M.-G. Suh and K. J. Vahala, Soliton microcomb range measurement, *Science* **359**, 884-887 (2018).

46. P. Trocha, M. Karpov, D. Ganin, M. H. P. Pfeiffer, A. Kordts, S. Wolf, J. Krockenberg, P. Marin-Palmo, C. Weimann, S. Randel, W. Freude, T. J. Kippenberg, and C. Koos, Ultrafast optical ranging using microresonator soliton frequency combs, *Science* **359**, 887-891 (2018).

47. J. Riemensberger, A. Lukashchuk, M. Karpov, W. Weng, E. Lucas, J. Liu, and T. J. Kippenberg, Massively parallel coherent laser ranging using a soliton microcomb, *Nature* **581**, 164-170 (2020).

48. Y. Li, S.-W. Huang, B. Li, H. Liu, J. Yang, A. K. Vinod, K. Wang, M. Yu, D.-L. Kwong, H. Wang, K. K.-Y. Wong, and C. W. Wong, Real-time transition dynamics and stability of chip-scale dispersion-managed frequency microcombs, *Light: Sci. Appl.* **9**, 52 (2020).

49. Y.-S. Jang and S.-W. Kim, Compensation of the refractive index of air in laser interferometer for distance measurement: A review, *Int. J. Precis. Eng. Manuf.* **18**, 1881-1890 (2017).

50. J. Schwider and J. Zhou, Dispersive interferometric profilometer, *Opt. Lett.* **19**, 995-997 (1994).

51. A. F. Fercher, C. K. Hitzenberger, G. Kamp, and S. Y. El-Zaiat, Measurement of intraocular distances by backscattering spectral interferometry, *Opt. Commun.* **117**, 43-48 (1995).

52. S.-W. Huang, J. Yang, M. Yu, B. H. McGuyer, D.-L. Kwong, T. Zelevinsky, and C. W. Wong, A broadband chip-scale optical frequency synthesizer at 2.7×10^{-16} relative uncertainty, *Sci. Adv.* **2**, e1501489 (2016).

53. P. Del'Haye, O. Arcizet, A. Schliesser, R. Holzwarth, and T. J. Kippenberg, Full stabilization of a microresonator-based optical frequency comb, *Phys. Rev. Lett.* **101**, 053903 (2008).

54. Z.L. Newman, V. Maurice, T. Drake, J.R. Stone, T.C. Briles, D.T. Spencer, C. Fredrick, Q. Li, D. Westly, B. R. Ilic, B. Shen, M.-G Suh, K.Y. Yang, C. Johnson, D.M.S. Johnson, L. Hollberg, K. J. Vahala, K. Srinivasan, S.A. Diddams, J. Kitching, S.B. Papp, and M.T. Hummon, Architecture for the photonic integration of an optical atomic clock, *Optica* **6**, 680-685 (2019)

55. J. Lim, A. A. Savchenkov, E. Dale, W. Liang, D. Eliyahu, V. Ilchenko, A. B. Matsko, L. Maleki, and C. W. Wong, Chasing the thermodynamical noise limit in microresonators for ultrastable laser frequency stabilization, *Nat. Comm.* **8**, 8 (2017).

56. J. Lim, W. Liang, A. B. Matsko, L. Maleki, and C. W. Wong, Probing 10□μK stability and residual drifts in the cross-polarized dual-mode stabilization of single-crystal ultrahigh-Q optical resonators, *Light: Sci. Appl.* **8**, 1 (2019).

57. See Supplemental Material [url] for detailed examinations, which includes Refs. [58-80].

58. K. E. Webb, J. K. Kang, J. Anthony, S. Coen, M. Erkintalo, and S. G. Murdoch, Measurement of microresonator frequency comb coherence by spectral interferometry, *Opt. Lett.* **41**, 277 (2016).

59. T. Kippenberg, R. Holzwarth, and S. Diddams, Microresonator-based optical frequency combs, *Science* **332**, 555–559 (2011).

60. V. Brasch, M. Geiselmann, T. Herr, G. Lihachev, M. Pfeiffer, M. Gorodetsky, and T. Kippenberg, Photonic chip–based optical frequency comb using soliton Cherenkov radiation, *Science* **351**, 357 (2016).

61. D. Cole, E. Lamb, P. DelHaye, S. A. Diddams, and S. Papp, Soliton crystals in Kerr resonators, *Nat. Photon.* **11**, 671 (2017).

62. Q. F. Yang, X. Yi, K. Y. Yang, and K. Vahala, Stokes solitons in optical microcavities, *Nat. Phys.* **13**, 53 (2016).

63. J. Jin, Y.-J. Kim, Y. Kim, S.-W. Kim, and C.-S. Kang, Absolute length calibration of gauge blocks using optical comb of a femtosecond pulse laser, *Opt. Express* **14**, 5968 (2006).

64. G. Wu, L. Liao, S. Xiong, G. Li, Z. Cai, and Z. Zhu, Synthetic wavelength interferometry of an optical frequency comb for absolute distance measurement, *Sci. Rep.* **8**, 4362 (2018).

65. K. G. Larkin, Efficient nonlinear algorithm for envelope detection in white light interferometry, *J. Opt. Soc. Am. A* **13**, 832 (1996).

66. C. Dorrer, N. Belabas, J.-P. Likforman, and M. Joffre, Spectral resolution and sampling issues in Fourier-transform spectral interferometry, *J. Opt. Soc. Am. B* **17**, 1795 (2000).

67. S. A. van den Berg, S. van Eldik, and N. Bhattacharya, Mode-resolved frequency comb interferometry for high-accuracy long distance measurement, *Sci. Rep.* **5**, 14661 (2015).

68. B. K. Kim and K.-N. Joo, A multi-channel fiber optic proximity sensor, *Meas. Sci. Technol.* **27**, 035104 (2016).

69. J. Park, J. Jin, J.-A. Kim, and J. W. Kim, Absolute distance measurement method without a non-measurable range and directional ambiguity based on the spectral-domain interferometer using the optical comb of the femtosecond pulse laser, *App. Phys. Lett.* **109**, 244103 (2016).

70. K.-N. Joo, Y. Kim, and S.-W. Kim, Distance measurements by combined method based on a femtosecond pulse laser, *Opt. Express* **16**, 19799-19806 (2008).

71. S. Han, Y.-J. Kim, and S.-W. Kim, Parallel determination of absolute distances to multiple targets by time-of-flight measurement using femtosecond light pulses, *Opt. Express* **23**, 25874-25882 (2015).

72. H. Zhou, Y. Geng, W. Cui, S.-W. Huang, Q. Zhou, K. Qiu, and C. W. Wong, Soliton bursts and deterministic dissipative Kerr soliton generation in auxiliary-assisted microcavities, *Light: Sci. & Appl.* **8**, 50 (2019).

73. P. Del'Haye, S. B. Papp, and S. A. Diddams, Hybrid electro-optically modulated microcombs, *Phys. Rev. Lett.* **109**, 263901 (2012).

74. D. Voigt, J. D. Ellis, A. L. Verlaan, R. H. Bergmans, J. W. Spronck, and R. H. Munnig Schmidt, Toward interferometry for dimensional drift measurements with nanometer uncertainty, *Meas. Sci. Technol.* **22**, 094029 (2011).

75. R. J. Jones, I. Thomann, and J. Ye, Precision stabilization of femtosecond lasers to high-finesse optical cavities, *Phys. Rev. A* **69**, 051803 (2004).

76. T. M. Fortier, M. S. Kirchner, F. Quinlan, J. Taylor, J. C. Bergquist, T. Rosenband, N. Lemke, A. Ludlow, Y. Jiang, C. W. Oates, and S. A. Diddams, Generation of ultrastable microwaves via optical frequency division, *Nat. Photon.* **5**, 425 (2011).

77. G. Tang, X. Qu, F. Zhang, X. Zhao, and B. Peng, Absolute distance measurement based on spectral interferometry using femtosecond optical frequency comb, *Opt. Lasers Eng.* **120**, 71-78 (2019).

78. P. E. Ciddor, Refractive index of air: new equations for the visible and near infrared, *Appl. Opt.* **35**, 1566–1573 (1996).

79. G. Wu, M. Takahashi, K. Arai, H. Inaba, and K. Minoshima, Extremely high-accuracy correction of air refractive index using two-colour optical frequency combs, *Sci. Rep.* **3**, 1894 (2013).

80. K. Jung, and J. Kim, Characterization of timing jitter spectra in free-running mode-locked lasers with 340 dB dynamic range over 10 decades of Fourier frequency, *Opt. Lett.* **40**, 316 (2015).

Figures and Tables

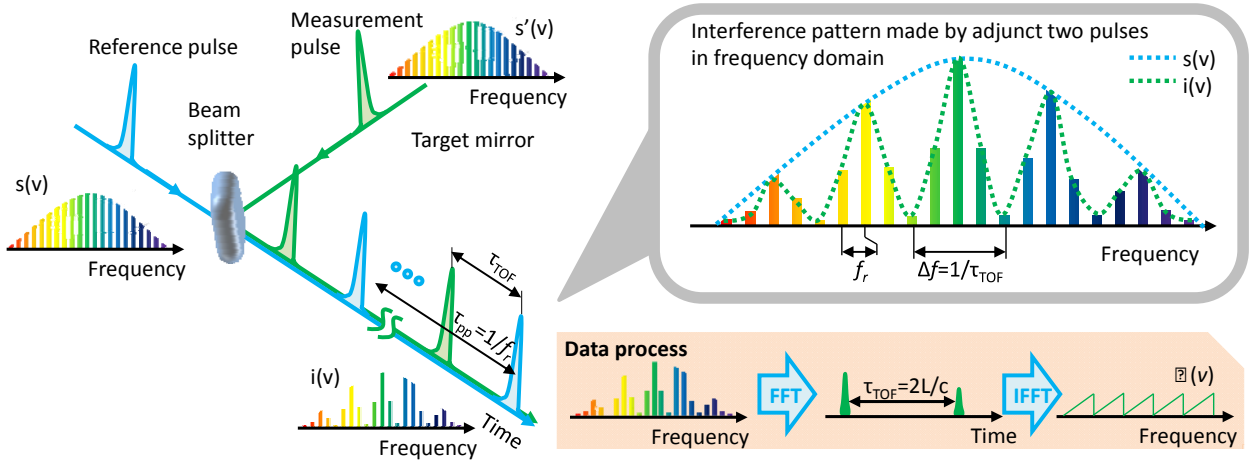

FIG. 1. Architectural approach of the spectrally-resolved ranging via soliton microcomb. Reference and measurement pulses of the soliton frequency comb, separated by τ_{TOF}. The measurement pulse has a relative phase shift □(ν) [= $2\pi\nu \times \tau_{TOF}$] to the reference pulse, and it makes an interference in every frequency mode of the soliton frequency comb. The information of τ_{TOF} is thus engraved on the interference pattern in the frequency domain, monitored via the spectrometer. The wide free-spectral range of frequency microcombs enables its comb-tooth resolved spectral interferogram to be directly readout by readily-available optical spectrum analyzers.

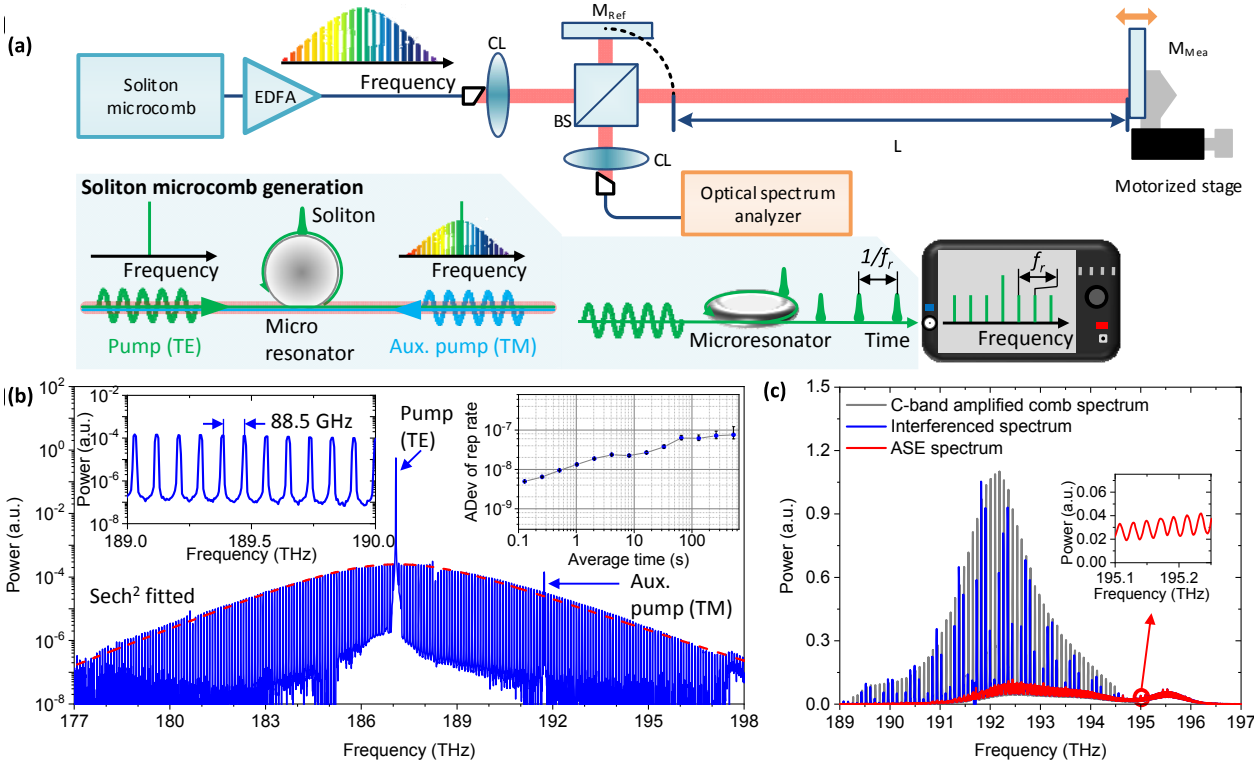

FIG. 2. Soliton microcomb-based precision dimensional metrology. (a) Soliton microcomb-based precision dimensional metrology via spectrally-resolved interferometry. BS: non-polarizing beam splitter, M_{REF}: reference mirror, M_{MEA}: measurement mirror, EDFA: erbium-doped fiber amplifier, CL: free-space collimator lens. Left inset describes schematic for the TE-TM dual-pumped soliton microcomb generation. (b) Example optical spectrum of the soliton microcomb from the high-Q Si_3N_4 microresonator, with the hyperbolic secant-square spectrum. Left inset: zoom-in illustration of the comb-tooth resolved spectrum. Right inset: Frequency stability of free-running repetition rate (f_r). (c) Example measured high-coherence spectral interferogram (blue) from the reference and measurement pulses, along with the superimposed spectra of the C-band amplified soliton microcomb (gray). Red line shows the amplified spontaneous emission (ASE) noise induced by the EDFA from the same spectral interferogram of the blue line. Inset: zoom-in illustration of the low-coherence ASE spectral interferogram with the low-visibility interference.

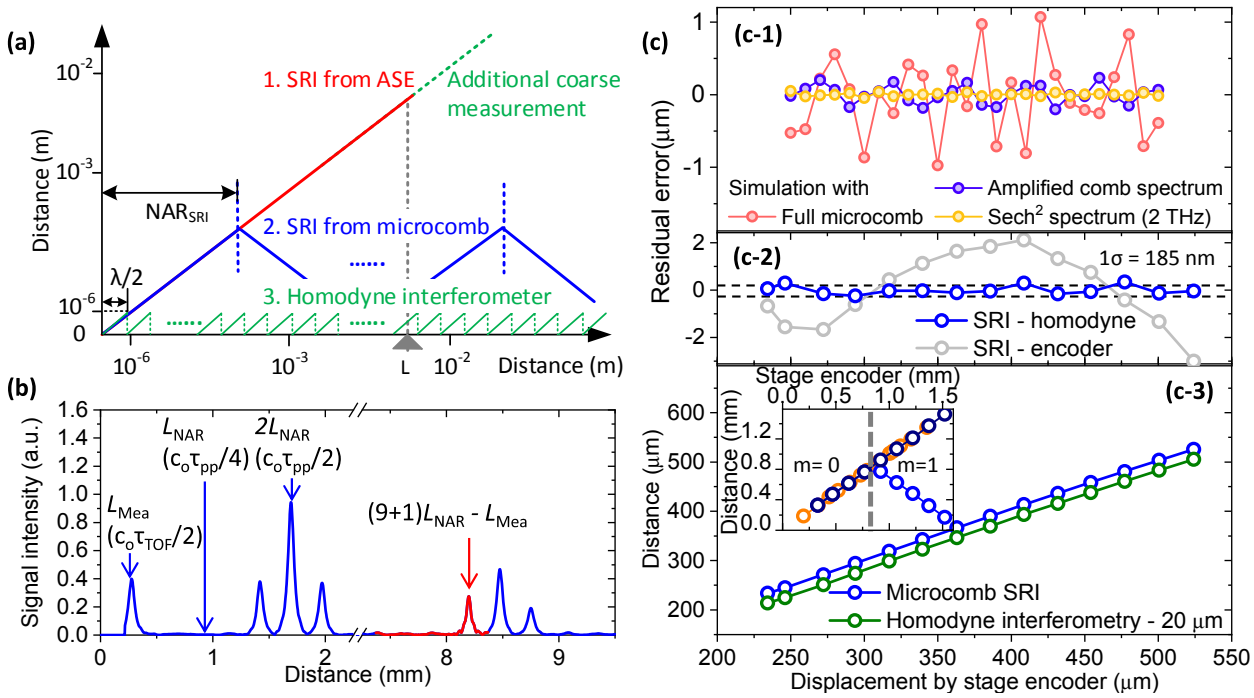

FIG. 3. Measurement linearity and distance measurement beyond the non-ambiguity range. (a) Non-ambiguity range extension by the combined platform of ASE-noise-based spectral interferometry, soliton microcomb spectral interferometry and homodyne interferometry. To determine integer M of the homodyne interferometry, the coarse distance measurement from the microcomb (with $\lambda/2$, where $\lambda = c_o/v$.) is used. At the same time, to determine integer m of the microcomb, the ASE SRI is used. (b) Time-domain signal reconstruction from the frequency domain interference. A typical signal-to-noise ratio of the time-domain signal is larger than 100. (c) Measurement linearity is evaluated by measuring the target distance with 25-μm incremental translation of a motorized stage. Top panel is the modeled results of positioning error for different spectral shapes. Middle panel is the residual error comparing SRI, homodyne interferometry and the encoder. Bottom panel left inset shows the measured distance beyond the non-ambiguity range. The wrapped distance (light blue) is unwrapped with calculated non-ambiguity in dark blue color. For comparison, a distance measurement from fiber-comb based spectrally-resolved interferometry is also plotted in orange color.

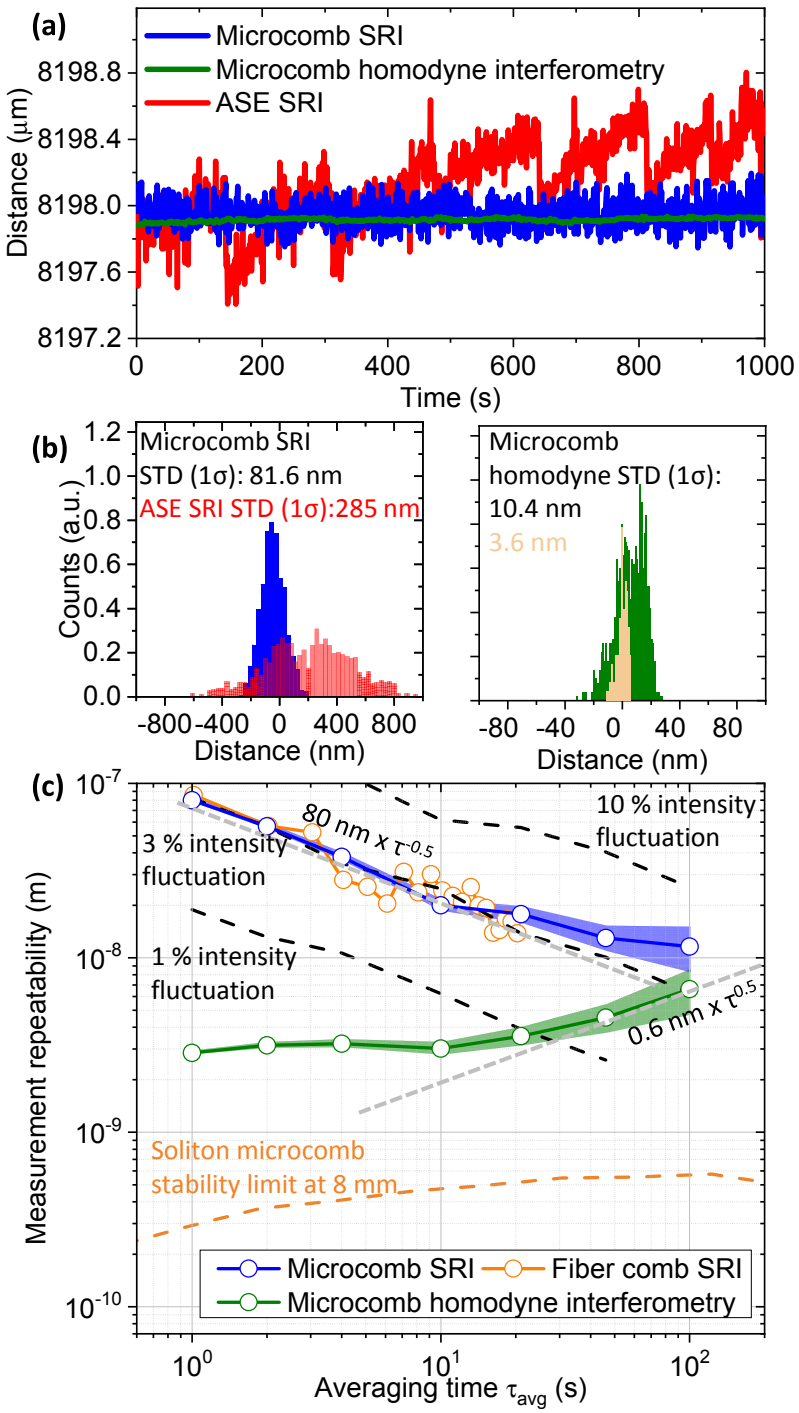

FIG. 4. Nanometer-scale precision distance measurement: reliability and repeatability evaluation. (a) Long-term distance metrology sampled over 1,000-seconds. (b) Left figure: histogram distribution of microcomb spectral interferometry and ASE spectral interferometry, with 1σ standard deviation of 81.6-nm (blue) and 285-nm (red) at 1,000-seconds measurement. Right: histogram distribution of homodyne interferometry, with 1σ standard deviation of 10.4-nm at 1,000-seconds measurement (green color). The 3.6-nm standard deviation is an example obtained

from 900 to 1,000-seconds (yellow color). (c) Measurement repeatability verification through Allan deviation of the long-term ranging data. 3-nm measurement repeatability is achieved from drift-compensated homodyne interferometry. The white noise limit is denoted by the dashed gray line while flicker noise is not observed within our 100-seconds averaging time. Measurements from a few-Hz-stabilized fiber mode-locked laser frequency comb laser metrology are illustrated for comparison. Black dashed lines denote simulation results about intensity fluctuation induced measurement repeatability. Orange dashed line denotes the free-running soliton microcomb frequency instability-induced measurement repeatability at 8 mm.